American Mineralogist, Volume 86, pages 47–54, 2001

An experimental study of the external reduction of olivine single crystals

LAURENCE LEMELLE,[1,*] FRANÇOIS GUYOT,[1,2] HUGUES LEROUX,[3] AND GUY LIBOUREL[4]

[1]Laboratoire de Minéralogie et Cristallographie de Paris, case 115, 4 place Jussieu, 75252 Paris, France
[2]Département des géomatériaux, Institut de Physique du Globe de Paris, 4 place Jussieu, 75252 Paris cedex 05, France
[3]Laboratoire Structure et Propriétés de l'Etat Solide, (ESA 8008), Université Sciences et Technologies de Lille, 59655 Villeneuve d'Ascq-Cedex, France
[4]Centre de Recherches Pétrographiques et Géochimiques (CRPG), Vandoeuvre-lès-Nancy, France

ABSTRACT

Single crystals of San Carlos olivine in contact with graphite were annealed at $P = 1$ bar, $T = 1373$ K, for studying the reaction of extraction of (Fe, Ni) metal. Scanning electron microscopy and transmission electron microscopy were performed on samples recovered after the experiments. Precipitates of (Fe, Ni) and thin amorphous layer of silica were identified, exclusively on the surface of the single crystals. Mass balance indicates that volatilization of Fe, Mg, and Si is negligible under these conditions. The reaction can be summarized as:

$$Fe_2SiO_{4\ \text{in olivine}} + 2C_{\text{graphite}} = 2Fe_{\text{in metal}} + SiO_{2\ \text{amorphous}} + 2CO_{\text{in gas}}$$

which occurs at the crystal surface without affecting the interior of the crystal, except for an Fe^{2+} and Mg^{2+} compositional profile in the olivine matrix. These chemical profiles are consistent with measured values of Fe^{2+}-Mg^{2+} interdiffusion coefficients, in agreement with the fact that Si and O are relatively immobile in olivine under such conditions.

This study shows that annealing at relatively moderate temperature under reducing conditions can cause surface modifications and thus probably can strongly influence the surface evolution of planetary objects exposed directly to space environments (regoliths, surfaces of asteroids, or interplanetary dust particles).

INTRODUCTION

The reaction that describes reduction of olivine can be written schematically as:

$$Fe_2SiO_{4\ \text{in olivine}} = 2Fe_{\text{in metal}} + SiO_{2\ \text{in silicate}} + O_2 \quad (1)$$

in which SiO_2 is either in a pyroxene, an amorphous silicate, or a melt. Olivine is an ubiquitous phase found in chondrites, interplanetary dust particles, stellar and interstellar environments, differentiated meteorites, and planets. Exposure of olivine to high-temperature reducing conditions, imposed by graphite or other carbonaceous phases (Boland and Duba 1981; Connolly et al. 1996; Bradley 1994; Sandford 1996; Hanon 1998), may occur in these environments, leading reaction 1 to have geochemical and cosmochemical importance. Indeed, microstructures likely associated with reduction processes of Fe^{2+} silicates have been identified in numerous cosmochemical environments: ureilite meteorites (Goodrich 1992; Berkley et al. 1980; Mittlefehldt et al. 1998), "dusty olivines" of chondrites (Rambaldi 1981; Nagahara 1981; Jones and Danielson 1997), and lunar regolith (Allen et al. 1993; Keller and McKay 1997). The study of reaction products of reaction 1 may therefore be useful in identifying reduction processes effectively occurring in planetary materials.

Reduction of olivine according to reaction 1 has been reported by several authors at $T \geq 1473$ K: metal precipitates and pores were observed by transmission electron microscopy (TEM) within bulk olivine (Boland and Duba 1986). These microstructures also were studied by optical microscopy (Boland and Duba 1986), scanning electron microscopy (SEM) (Connoly et al. 1994), and electron microprobe analysis (Lemelle 1998; Lemelle et al. 2001). Reaction mediated by a gas phase between olivine and metal was investigated using Kudsen-cell mass spectrometry (Dohmen et al. 1998). At temperatures below 1473 K, however, microstructures have not yet been studied; the most documented study reports enrichment in Si and O a few micrometers below the surface of olivine annealed at various values of oxygen fugacity (Jaoul et al. 1987) and measured by Rutherford backscattering spectroscopy (RBS). In this study, we document by SEM and TEM the microstructures of natural San Carlos olivine single crystals in contact with graphite, annealed at $T = 1373$ K and $P = 1$ bar total pressure for different durations. Similarities with micro-

* Present address: Laboratoire de Sciences de la Terre, ENS Lyon, 46 allée d'Italie, 69364 Lyon cedex 07, France. E-mail llemelle@ens-lyon.fr

structures observed in lunar regolith, interstellar dust particles (IDP), "dusty" olivines, and ureilites are briefly discussed.

EXPERIMENTAL METHODS

We used gem quality single crystals of San Carlos olivine, optically free of impurities. Chemical compositions, analyzed by electron microprobe, are given in Table 1. Oriented slices were cut with dimensions of 1.8 mm × 2.2 mm × 0.7 mm, with the main crystal surface parallel to either (001) or (010), using the *P*bnm configuration of space group no. 62 for olivine. The sections were polished, with the final polish performed using 0.25 µm diamond paste. Special care was taken to verify that, prior to the reduction reaction, the crystal surfaces were composed of pure olivine. Etching by hydrofluoric acid was not performed because its chemical effects on olivine have not yet been well characterized.

The samples were annealed at T = 1373 K in a vertical muffled tub furnace at CRPG, for durations ranging between 2.5 h and 48 h. A summary of the run conditions is given in Table 2. The single crystals were seated in a pure graphite crucible, and were surrounded by graphite powder. Pure CO gas was flushed through the furnace at 300 mL/min during the experiment. At the end of the experiments, samples were quenched by dropping them into a receptacle at ambient temperature, under pure CO atmosphere.

TABLE 1. Chemical composition of San Carlos olivine

elements	(1)	(2)	(3)	(4)	(5)	(6)
Fe	7.36	2.77	0.04	2.81	0.07	0.04
Mg	29.76	25.74	0.7	25.55	0.21	0.26
Si	18.99	14.26	0.1	14.31	0.12	0.16
Ni	0.3	0.10	0.02	0.10	0.02	0.01
O	43.45	57.11	0.2	57.16	0.06	0.6
Sum	99.86			99.93		

Note: (1) Average composition in wt% of 15 AEM analyzes, (2) Atomic composition corresponding to column 1, (3) Standard deviations for column 2, (4) Average composition analyzed in at% of 23 ATEM analyzes, (5) Standard deviations for column 4, (6) Error bars calculated on the basis of statistical precision for column 4.

TABLE 2. Summary of the experimental conditions and studied samples

	T = 1373 K
$\log f_{O_2}$(bar) $_{eq}$*	–15.75
$\log f_{O_2}$(bar) $_{eq\ 1000ppmNi}$†	–13
$\log f_{O_2}$(bar) experimental	–17.65
$\log f_{O_2 eq}$-$\log f_{O_2}$exp	1.9
$\log f_{O_2 eqNi}$-$\log f_{O_2}$exp	4.65
A (KJ/mol)‡	49.9
$A_{1000\ ppmNi}$ (KJ/mol)	122.2
flux of CO (mL/min)	300
t = 2.5 h	no. 1 (010) and no. 6 (001)§
t = 5 h	no. 2 (010)II and no. 7 (001)
t = 13 h	no. 3 (010)II and no. 8 (001) II
t = 24 h	no. 4 (010)II and no. 9 (001)
t = 48 h	no. 5 (010) and no. 10 (001)

* Oxygen fugacity calculated at the limit of stability of an $Fo_{90}Fa_{10}$ olivine at P = 1 bar and T = 1373 K with respect to metal precipitation.
† Oxygen fugacity calculated at the limit of stability of an $Fo_{90}Fa_{9.9}$ olivine with 0.1 at % Ni_2SiO_4 at P = 1 bar and T = 1373 K with respect to metal precipitation.
‡ Affinity at P = 1 bar of the solid-state reduction reaction of a $Fo_{90}Fa_{10}$ olivine into metal and quartz: $A = -RT\ln\left[\frac{f_{O_2\ experimental}}{f_{O_2\ equilibrium}}\right]$.
§ Crystalline orientation (using the *Pbnm* configuration) of the olivine surface exposed to the gas mixture for a given annealing duration and sample numbers.
|| Samples studied by TEM.

Zirconia f_{O_2} sensors are unstable under such highly reducing conditions. We assumed that f_{O_2} was fixed at the solid-gas C/CO buffer. The f_{O_2} calculated for the C/CO buffer at T = 1373 K is $10^{-17.65}$ bar (Deines et al. 1974). Following Nitsan (1974), and using updated thermodynamic data (Fei and Saxena 1986; Holland and Powell 1990), the f_{O2} for olivine/metal equilibrium at T = 1373K in $(Mg_{0.9}Fe_{0.1})_2SiO_4$ is $10^{-15.7}$ bar (Table 2). This value is modified in natural olivine by the presence of 0.1 at% of Ni (see Table 1). Calculations taking into account the effect of Ni yield an equilibrium fugacity of 10^{-13} bar at T = 1373 K. The experimental f_{O_2} of the present study was therefore well below the equilibrium fugacity between San Carlos olivine and (Fe,Ni) metal, by more than 4 log units (see Table 2). The calculated $[Fe^{2+}/(Fe^{2+} + Mg^{2+})]$ of olivine in equilibrium with the external atmosphere in these experiments is 0.01.

Recovered samples were studied by SEM and TEM. SEM analyses were performed with a Stereoscan 440 (Leo) operated at 20 kV equipped with a Si(Li) diode for energy-dispersive X-ray microanalysis (EDX). Samples selected for TEM were thinned on the internal crystal sides, while the external reaction surfaces were protected. Thinning was performed mechanically down to 20 µm thickness, and then ion milling was carried out down to electron transparency with a precision ion-polishing system (PIPS). For establishing compositional profiles by analytical TEM, transverse cuts of the samples were prepared and thinned by ionized Ar gas. TEM studies were carried out with a Philips CM 30 operated at 300 kV, using a Noran-Voyager EDX analytical attachment equipped with a Ge diode having an ultra-thin window. This equipment allows the detection of low energy characteristic X-ray lines such as the O_K line (0.523 kV) with a good sensitivity. The Cliff and Lorimer factors were determined by the parameterless method of Van Cappellen (1990) using standard specimens. The absorption corrections were applied using the method proposed by Van Cappellen and Doukhan (1994). These authors have shown that the thickness of the analyzed zone can be deduced from EDX spectra by comparing the intensity of the O_K emission line to those of the different cations and assuming electrical neutrality.

RESULTS

A typical secondary electron SEM image of the olivine surface after annealing is shown in Figure 1. The two most prominent features are Fe-rich precipitates distributed homogeneously on the surface, and steps regularly spaced on the olivine surface. The precipitates, everywhere smaller than 1 µm, appear in relief and are located exclusively at the surface. SEM and TEM studies of transverse cuts show their absence in the crystal interior. The precipitates are faceted (Fig. 1 and Fig. 2a), and these facets have a common orientation. In some cases, it is possible to observe an acute angle at the contact between the surface and the precipitate (Fig. 1). The metal phase is always bcc-Fe. The precipitates are Fe-rich with Ni as a minor component; Co and P also have been detected (see Table 3). They do not display noticeable compositional variations and they are not chemically zoned. Very few dislocations have been found

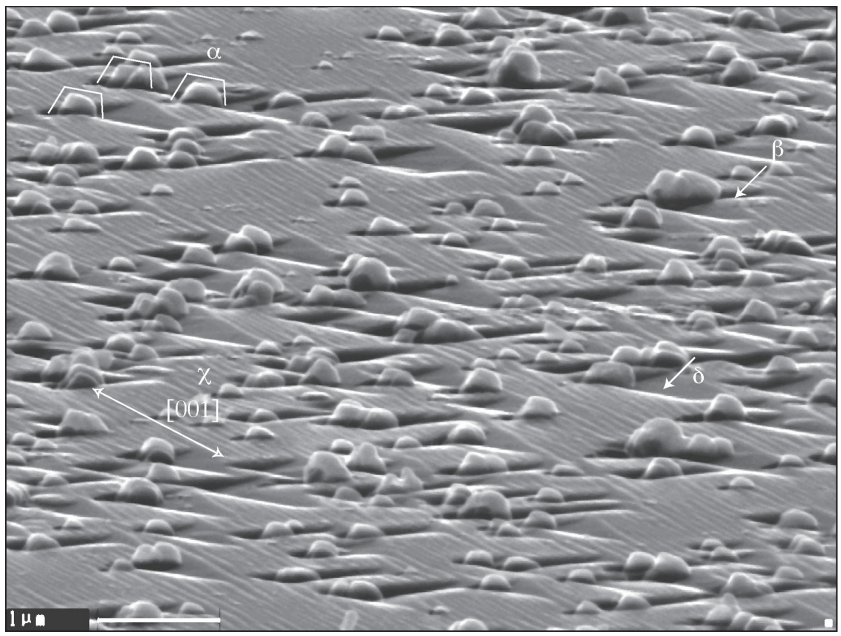

FIGURE 1. Secondary electron (SE) image of the surface of sample no. 3 annealed for 13 h at T = 1373 K, (tilt angle of 80°). Symbols correspond to details described in the text: α = common distribution of facets of precipitates, β = acute angle between surface and precipitate, χ = crystallographic orientation of steps, δ = depressed area free of steps. Scale bar = 1 µm.

TABLE 3. ATEM chemical compositions of precipitates of sample no. 8 annealed fov 13 h

Precipitate*	Fe at%	Ni at%	Co at%	P at%	S at%
1	92.51	3.95	0.26	2.90	0.38
1	93.10	3.46	0.18	2.70	0.56
1	92.95	4.02	0.41	2.41	0.21
2	92.88	3.73	0.39	2.57	0.17
2	93.32	3.31	0.31	2.38	0.35
2	93.13	3.56	0.37	2.30	0.46
3	93.11	3.35	0.46	2.51	0.34
4	93.59	3.27	0.37	2.52	0.26
5	93.47	3.55	0.30	2.37	0.10
6	93.31	3.70	0.28	2.43	0.06
at%†	93.14	3.59	0.33	2.51	0.29
ε (at%) ‡	(0.6)	(0.2)	(0.2)	(0.16)	(0.12)
σ (at%) §	[0.30]	[0.25]	[0.08]	[0.17]	[0.15]

* Precipitate number.
† Average composition.
‡ Error bars of average composition, calculated on the basis of statistical precision of analyzes.
§ Standard deviation of average composition.

in neighboring olivine (Fig. 2a), and they have no apparent relationship to the precipitates. The steps on the olivine surface are characterized by edges oriented along [001] on (010) and [100] on (001). The steps are regularly distributed on the surface, except near precipitates where a depressed area, apparently free of steps, is visible on the same side of all precipitates (Fig. 1). As checked by TEM, the surface of this depressed area is either (010) or (001).

Backscattered electron (BSE) images are given in Figure 3 for different annealing times. Because of the strong Z contrast between the metallic precipitates and the silicate matrix, the BSE images are suitable for image processing. After 2.5 h of annealing (Fig. 3a), very few precipitates are observed on the surfaces. After 5 hours (Fig. 3b), the number of precipitates has dramatically increased. Then, the number of precipitates per surface unit decreases whereas their size increases (Fig. 3c). Diameters of the projected surfaces of the precipitates (Ø, µm), number of precipitates per surface unit (ρ, 1/µm^2) and fraction of the silicate surface covered by the projected surface of the precipitates (∅, µm) have been calculated. The results of image processing, performed with the Imagenia 2000 software (version 2.0, BIOCOM), are given in Table 4. The number, size, and distribution of the metallic precipitates are strongly influenced by surface heterogeneities, such as scratches, inclusions (Fig. 4), or sub-grain boundaries. Such heterogeneities are probably very important in natural olivine, but for the sake of reproducibility, we purposely selected samples as free of heterogeneities as possible. Reduction results in both an increase of the total surface covered by metal, an increase in the size of precipitates, and a decrease of their number per surface unit. The reorganization of the precipitates is due to coalescence, coming from a redistribution of metallic Fe among the precipitates. The quasi-monomial distribution of sizes requires that the smallest precipitates disappear to form the biggest in an Ostwald ripening process on the surface.

Compositional profiles perpendicular to the sample surface were obtained by analytical TEM on transverse cuts, with a probe size of 15 ± 5 nm $\times$ 100 ± 5 nm and a minimum step size of 5 nm. To minimize electron beam broadening and to increase the analytical spatial resolution, we only recorded profiles on very thin areas (typically 50–100 nm thick). The profiles are insensitive to the position of the starting point at the surface. Deeper than 1 µm below the surface, the composition does not differ from that of the initial olivine (Table 1).

The profiles, from the interior to the surface (Fig. 5a), are first characterized by an increase in the Fe content of the olivine. Very near the surface (Fig. 5b), there is an increase in Si, a strong decrease in Mg and Fe, and an evolution of the O/Si

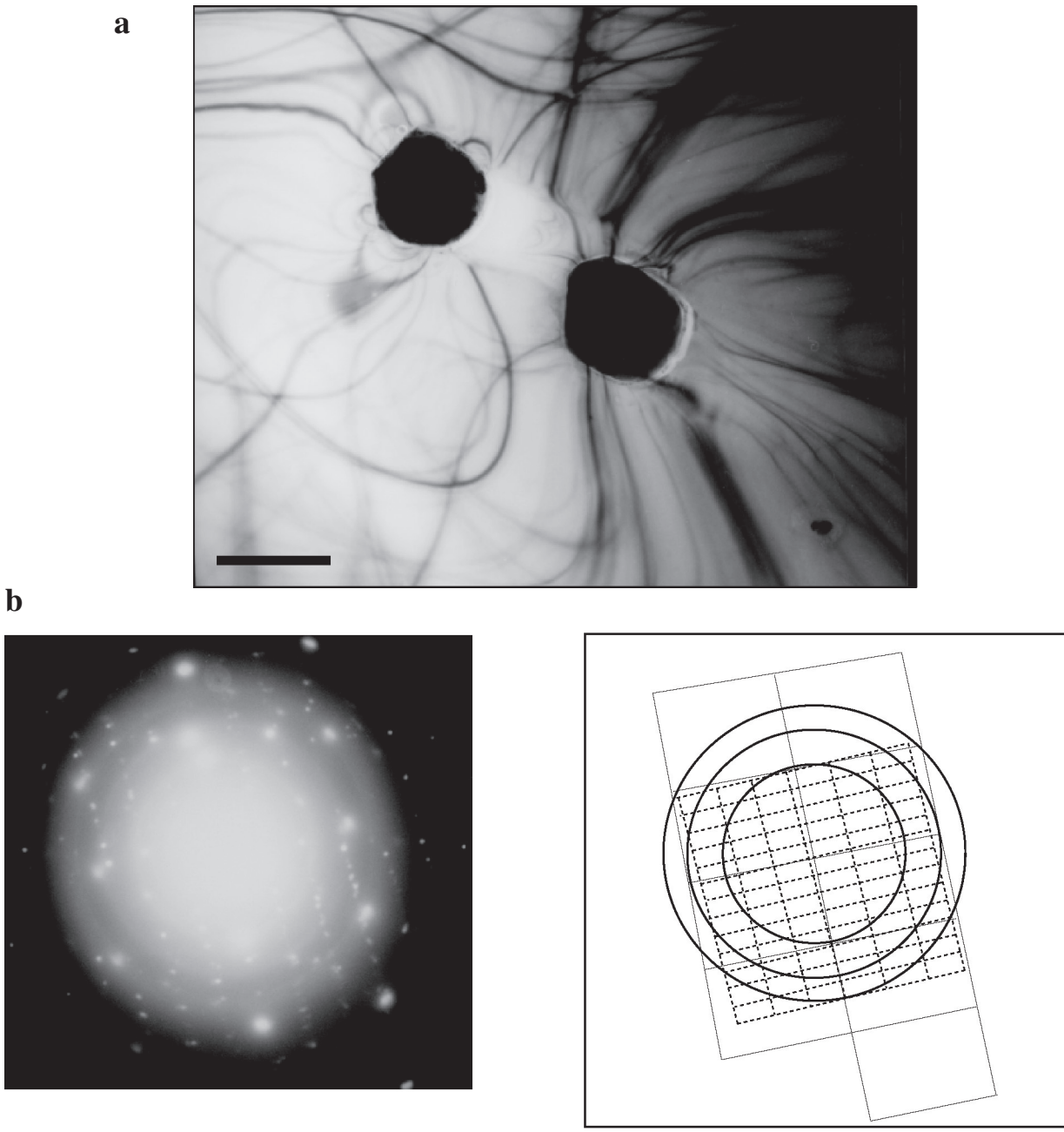

FIGURE 2. (**a**) TEM image of the surface of sample (no. 8) annealed during 13 h at $T = 1373$ K. Metallic precipitates appear in black. Scale bar = 750 nm. (**b**) Electronic diffraction micrograph of the assemblage shown in Figure 2a (left) with its representation (right).

ratio to values close to 2, revealing the presence of a silica-rich layer (SiO_2), covering the surface. The thickness of the SiO_2 layer was estimated at approximately 9 nm from analytical TEM performed on the planar view of the surface of the same sample. The systematic absence of diffraction spots different from those of olivine and metal shows that this SiO_2 layer is amorphous (Fig. 2b). Fourier transform transmission infrared spectroscopy of powders [experimental procedure given in Lemelle (1998)] also shows increasing abundance of amorphous SiO_2 as the reduction of olivine proceeds.

Regardless of any hypothesis on the mechanism producing the compositional gradients, the observed Mg^{2+}-Fe^{2+} profiles (Fig. 5a), and thus the integrated amount of Fe^{2+} extracted from the olivine, can be estimated numerically (Fig. 5a and Table 4). Within the precision of the calculation, the extracted amount of Fe^{2+} and the amount of Fe^0 present on the surface are equal (Table 4), indicating that no significant amount of metal has been vaporized. The amount of surface silica can be estimated from the ~9 nm thickness of the amorphous SiO_2 layer (Fig. 4b) using the density of quartz as a proxy. We find that the

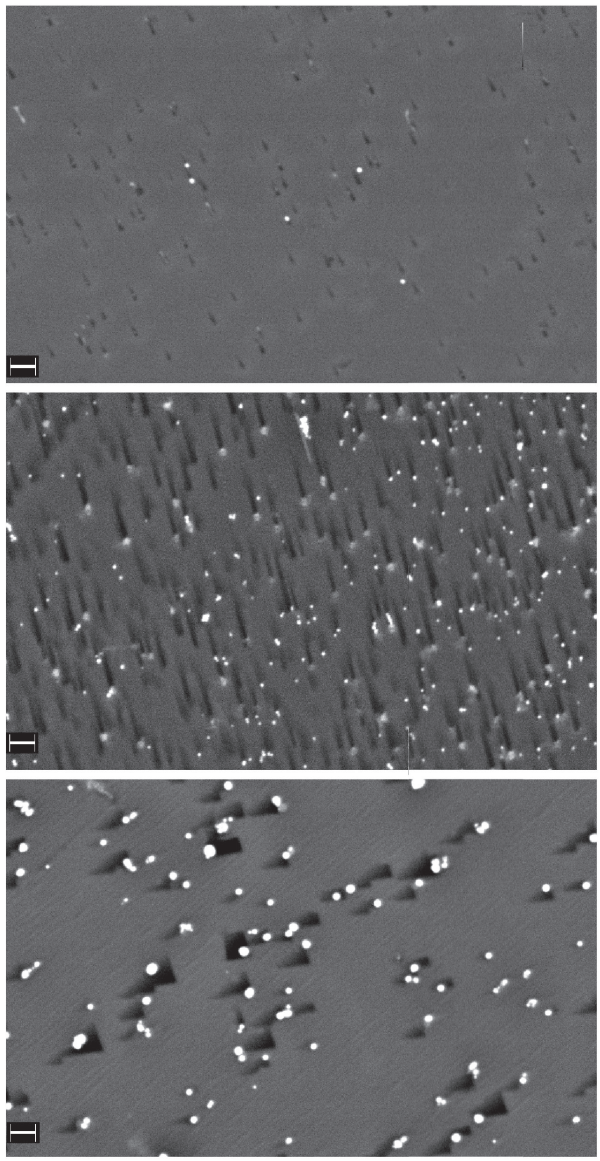

FIGURE 3. Backscattered electron (BSE) images of the surface of samples annealed at T = 1373 K for run duration t = 2.5 h (no. 1 in Fig. 3a), t = 5 h (no. 2 in Fig. 3b), t = 13 h (no. 3 in Fig. 3c). Scale bar = 1 μm.

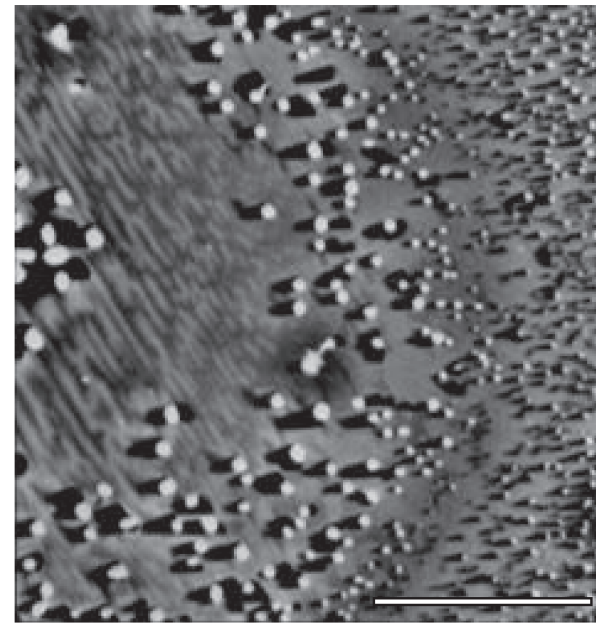

FIGURE 4. BSE image of a surface stained by an inclusion enriched in Ca in a sample annealed for 13 h at T = 1373 K. Metallic precipitates are the bright spots. Scale bar = 8 μm.

TABLE 4. Geometrical characteristics of the surface metal precipitates

	t = 5h	t = 13h
Ø * (μm)	0.14	0.37
ρ† (1/μm²)	0.63	0.22
S‡ (%)	1	2.8
n_{Fe}^{0} § (mol/μm²)	1.2±4 10^{-16}	7.8 ± 4 10^{-16}
n_{Fe}^{2+} ‖ (mol/μm²)	–	10 ± 2 10^{-16}
$n_t^{no.}$ (mol/μm²) (see text)	3.4 ± 0.3 10^{-16}	11 ± 0.3 10^{-16}

* Average diameter of precipitates.
† Density of precipitates.
‡ Surface fraction recovered by metal precipitates.
§ Number of moles of metal per surface unit using: $n_{Fe^0} = \left(\frac{4}{3}\pi\left(\frac{\varnothing}{2}\right)^3\right)\left(\rho\frac{d}{M}\right)$, with d the density and M the molar mass of bcc-Fe.
‖ Number of moles of FeO extracted from the bulk estimated from the compositional profile measured by ATEM on transverse cut (see Fig.5b) in the following way : $n_{Fe^{2+}}(\text{mol.nm}^{-2}) = \frac{100c_{Fe}}{2(\%_{Fa})_{+\infty}}\int_0^{1045} P(x)dx$ in which P(x) is a polynomial fit of the fayalite content reported in Figure 5a.
Number of moles of FeO extracted from the bulk estimated from Equation 3: $n_t = 2c_{Fe}(kt/\pi)^{1/2}$.

number of moles of silica at the surface (3.6 ± 0.8 10^{-16} mol/μm²) is half the number of moles of extracted Fe (see Table 4). The global mass balance therefore can be summarized schematically by the stoichiometric decomposition of the fayalite component of olivine as follows:

$$Fe_2SiO_{4\ \text{in olivine}} + 2C_{\text{graphite}} = 2Fe_{\text{in metal}} + SiO_{2\ \text{amorphous}} + 2CO_{\text{in gas}} \quad (2)$$

By this mass balance, and because the volatilization of metal is not significant, the system is closed for Fe and also for Mg and Si.

DISCUSSION

The microstructures observed in this study reveal that reduction proceeded through a surface reaction, as neither metal precipitates nor silica were observed in the bulk of the olivine crystals. On the olivine surface (Fig. 1), the formation of steps (or facets) is most likely related to a small misorientation between the initial polished olivine surface and the crystallographically dense planes (010) or (001). Indeed, the initial slightly misoriented surface is less stable than a surface con-

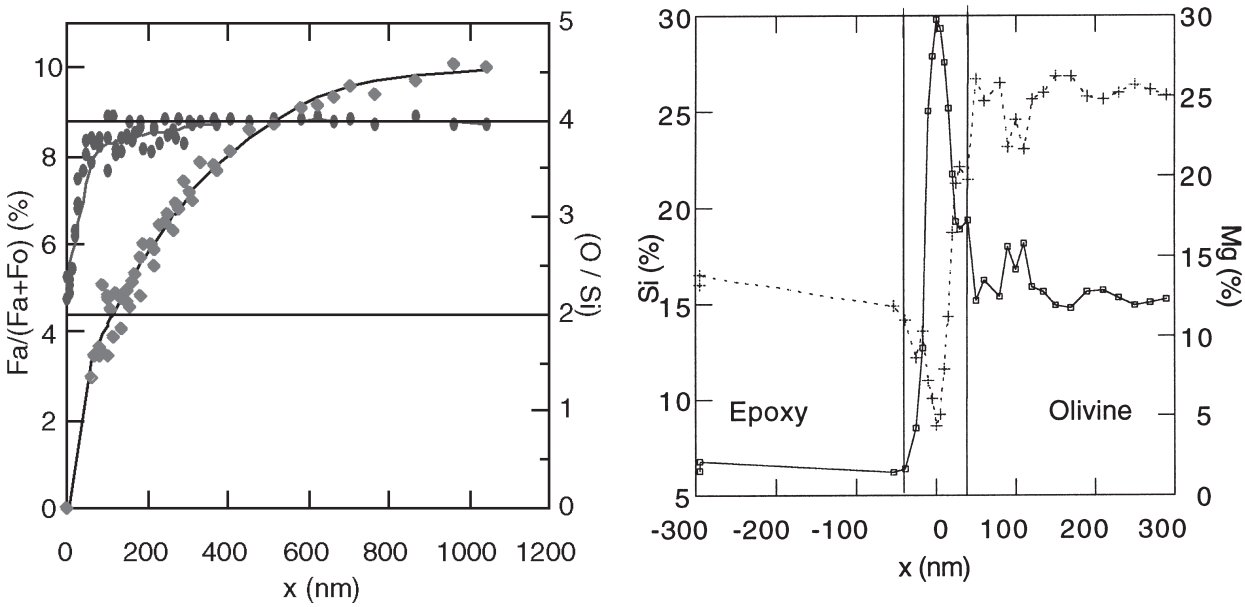

FIGURE 5. (**a**) Analytical TEM profiles of fayalite content, Fa/(Fa + Fo) (solid diamonds), and (O/Si) (solid circles) in a transverse cut of sample no. 3 annealed 13 h at T = 1373 K. These profiles result from the superposition of 3 profiles measured separately starting at the surface (x = 0). (O/Si) of olivine and quartz are marked by solid lines. (**b**) Analytical TEM composition profiles of Si (at%) (open squares) and Mg (at%) (crosses) in a transverse cut of sample no. 3 annealed 13 h at T = 1373 K. Domains of epoxy exist between the two surfaces of the transverse cut.

sisting of densely stepped planes. Steps are formed by surface diffusion induced by high surface energy of the initial surface. We observe that the terraces of steps get broader as annealing duration increases, which is a result of migration of the step edges on the surface. This migration strongly interacts with the metal precipitates, and might play a role in the mechanism of coalescence of precipitates. As shown in Figure 6, step edges are pinned on one side of the precipitates. Thus, the steps sweep unidirectionally across the surface, simultaneously with the growth of metal precipitates. Precipitates act as obstacles, which explains why the depressed zones with faceted edges appear only on one side of these precipitates. The composition of the metal phase (Table 3) can be explained by the coupled reduction of Fe, Ni, and Co from the initial olivine. Indeed, a simple mass-balance calculation indicates that reduction of 2.8 at% of Fe (Table 1), 1100 ppm of Ni (Table 1), and 100 ppm of Co from an initial olivine would produce the metal composition given in Table 3. These values are consistent with that usually measured in San Carlos olivines. The high P and S content recorded by the microanalysis probably come from the graphite (or from contamination during the annealing). However, it cannot be excluded that some P was in solid solution in the starting olivine, and was reduced during the annealing. Indeed, the presence of P in metal (coming from reduction process) in chondrites has been reported by Zanda et al. (1994). The metal phase is always recovered as bcc-Fe. According to the ternary Fe-Ni-P phase diagram at 1100 °C (Doan and Goldstein 1970), the metallic precipitates should be both bcc and fcc because their complex composition corresponds to the bcc+fcc binary field. We therefore conclude that either nucleation on olivine favors bcc-Fe at high temperature, or fcc-Fe could not be quenched and was converted into the bcc structure.

A topotaxial relation of precipitates on the dense planes of olivine is shown by the common orientations of their facets (Fig. 1) and by systematic crystallographic relations between diffraction patterns of olivine and metal (Fig. 2b). For both phases, the orientations of the planes of the facets represent easy growth planes, which explains the topotaxial relationships. If an fcc to bcc transformation occurred during the quench, topotaxial relations between olivine and metal must have been preserved through the transformation because of the close crystallographic relationships that prevail during this phase transformation: the fcc {111} planes are parallel to the bcc {110} planes.

In olivine there is no fast path for diffusion (e.g., cracks or grain boundaries) because the profiles are insensitive to the position of the starting point on the surface. In addition, such fast paths would generate, at their intercepts with the surface, inhomogeneities in the distribution and sizes of the metal precipitates. Such features are not observed, except in very rare cases related to micrometer-sized chemical impurities (Fig. 4).

The profile shown in Figure 3a can be described by the expression:

$$\%_{\mathrm{Fa}}(x) = \left(\%_{\mathrm{Fa}}\right)_{+\infty} \mathrm{erf}\left(\mathrm{x}/2\sqrt{\mathrm{k}t}\right) \qquad (3)$$

where x is the distance away from the surface; $\%_{\mathrm{Fa}}$(x) and $(\%_{\mathrm{Fa}})_{+\infty}$ represent the $[Fe^{2+}/(Fe^{2+} + Mg^{2+})]$ ratios at position x and in the initial olivine, respectively; t is the duration of reaction; and k is a constant that has the dimension of a diffusivity. The experimental and calculated profiles are given in Figure 7. The fitting parameter k in Equation 3 is close to the diffusivity D of Fe^{2+}-Mg^{2+} in olivine at T = 1373 K and $f_{O_2} = 10^{-17.65}$ bar

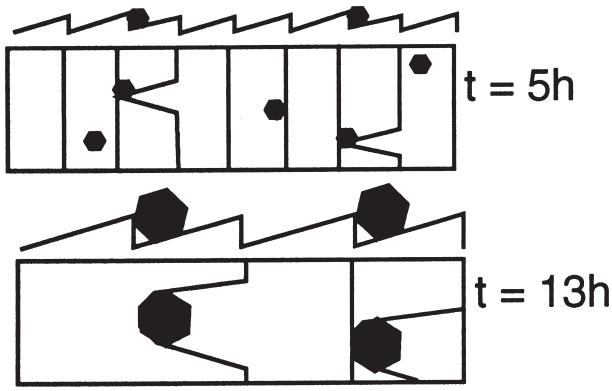

FIGURE 6. Schematic interpretation of surface topography of samples (planar and transverse views) in terms of interaction between unidirectional migration of steps and growth of precipitates. For explanations, see text.

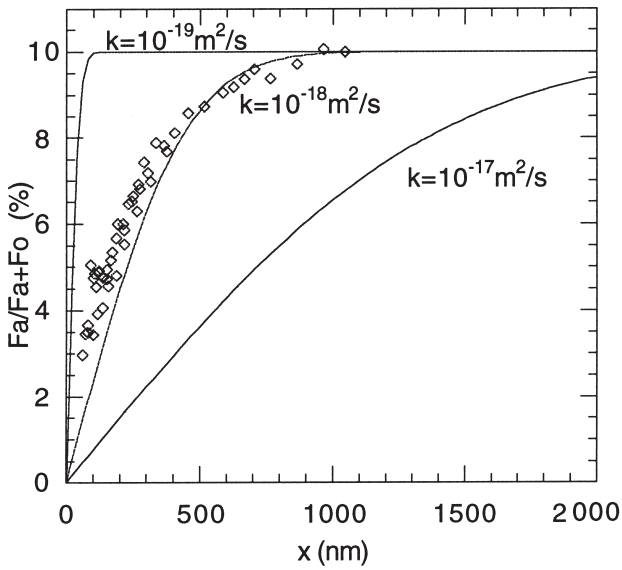

FIGURE 7. Comparison of the experimental profile (Fig. 5a) and theoretical profiles of Fe-Mg interdiffusion (solid lines) in olivine calculated from Equation 3 parameterized with different k values.

($10^{-18.5}$ m^2/s < $D_{Fe^{2+}\text{-}Mg^{2+}}$ < 5 $10^{-17.5}$ m^2/s) (Nakamura and Schmalzried 1984; Chakraborty 1997). The similarity of Equation 3 to an Fe^{2+}-Mg^{2+} interdiffusion profile in a semi-infinite medium is not unexpected. The metal extraction at the olivine surface generates a gradient of chemical potential of Fe^{2+} in the interior of the crystal beneath the surface, resulting in Mg^{2+}-Fe^{2+} interdiffusion profile (Fig. 5a). In addition, note that the effective value of k is smaller ($k = 5.6 \pm 0.5\ 10^{-19}$ m^2/s) near the FeO-free surface of olivine than in the bulk ($k = 1.1 \pm 0.1\ 10^{-18}$ m^2/s). Extrapolation of diffusivity measurements of Nakamura and Schmalzried (1984) to our experimental conditions predicts that D in pure forsterite should be two thirds of that in an olivine with 10% fayalite.

Effects of k variations on composition profiles were studied elsewhere with a finite difference model of the reduction of olivine at slightly different conditions (see Fig. 10 in Lemelle et al. 2001). Wu and Kohlstedt (1988), in their study of olivine oxidation, also showed the importance of Fe^{2+}-Mg^{2+} interdiffusion. In the case of oxidation, oxygen is added at the olivine surface resulting in an Mg-Fe-O layer because Mg^{2+} and Fe^{2+} are the fast ionic diffusing species in olivine. The propagation of defects modeled as divalent cationic vacancies and electronic holes in the olivine then results in an Fe^{2+}-Mg^{2+} gradient as well as in internal reaction products (magnetite and silica). In the present case of reduction, the slow-diffusing species, i.e., Si and O, also remain immobile compared with the fast-diffusing species Mg^{2+} and Fe^{2+}. This leads to the formation of metal precipitates and of a remaining Si, O layer at the olivine surface whereas the diffusion of divalent cation vacancies from the surface to the interior establishes the observed Fe^{2+}-Mg^{2+} gradient in the olivine. Except for the chemical profile, no reaction phenomenon is observed within olivine (i.e., no internal reaction occurs); under these experimental conditions, the reduction reaction remains an external reaction. For similar run duration and thermodynamic affinities, the case is different at higher temperatures (T > 1623 K) because short-circuit diffusion of Si and O enhances the transport of these elements from interior to surface, resulting in an internal reduction reaction with porosity (Lemelle 1998; Lemelle et al. 2001).

CONCLUDING REMARKS

Microstructures such as those observed in the present study could be present on Fe silicate grains in planetary material affected by reduction reactions. Indeed, reaction rims enriched in amorphous silica, commonly containing nanometer-sized metal precipitates, have been observed in lunar regolith grains (Keller and McKay 1997) and as "GEMS" (Glass Embedded Metal Sulfides) in anhydrous interplanetary dust particles (Bradley 1989, 1994). Processes involved in causing these nanostructures are still extensively debated, solar wind irradiation and/or volatilization being the most frequently proposed. The present study might be helpful for constraining further the environmental parameters that produced these microstructures. Fine-scale microstructures of reduced silicates have also been described extensively in meteorites: e.g., dusty olivines in chondrites and fine-grained graphite-metal assemblages surrounding silicate grains in ureilites. Formation of dusty olivines implies an internal reduction reaction of olivines, suggesting higher temperatures than in the present study, and has been discussed by Lemelle et al. (2001). In ureilites, the observed reduction microstructures develop on spatial scales between 10 and 100 μm and therefore imply either much longer time scales or more severe thermal conditions than in the present study (Lemelle et al. 2001). A detailed study, at the nanometer scale, of reduction rims and compositional profiles in ureilites remains, however, to be done to determine the conditions that prevailed during the formation of their reduction rims.

ACKNOWLEDGMENTS

We thank Stephan Borensztajn and Luc Beaunier (Physique des Liquides et Electrochimie) for SEM images and Alain Rouiller (CRPG) for his technical assistance during the experiments. We had numerous constructive discussions with Al Duba about the reduction experiments. The paper benefited consider-

ably from detailed reviews by Carlton Allen, Allan Treiman, John Jones, and Simon Sheppard—all of whom greatly improved the initial version. This research was supported by INSU-CNRS programs "Interieur de la Terre and Germ" and "Programme National de Planétologie".

REFERENCES CITED

Allen, C.C., Morris, R.V., Lauer, H.V. Jr., and MacKay, D.S. (1993) Microscopic iron metal on glass and minerals- a tool for studying regolith maturity. Icarus, 104, 291–300.

Berkley, J.L., Taylor, G.J., and Keil, K. (1980) The nature and origin of ureilites. Geochimica et Cosmochimica Acta, 44, 1579–1597.

Boland, J.N. and Duba, A. (1981) Solid-state reduction of iron in olivine, planetary and meteoritic evolution. Nature, 294, 142–144.

Boland, J.N. and Duba, A. (1986) An electron microscopy study of the stability field and degree of nonstochiometry in olivine. Journal of Geophysical Research, 91, 4711–4722.

Bradley, J.P., Germani, M.S., and Brownlee, D.E. (1994) Automated thin-film analyzes of anhydrous interplanetary dust particles in the analytical electron microprobe. Earth and Planetary Science Letters, 93,1–13.

Bradley, J.P. (1994) Nanometer-scale mineralogy and petrography of fine-grained aggregates an anhydrous interplanetary dust particles. Geochimica et Cosmochimica Acta, 58, 2123–2134.

Chakraborty, S. (1997) Rates and mechanisms of Fe-Mg interdiffusion in olivine at 980 °C–1300 °C, Journal of Geophysical Research, 102, 12317–12331.

Connolly, H.C., Hewins, R.H., Ash, R.D., Zanda, B., Lofgren, G.E., and Bourot-Denise, M. (1994) Carbon and the formation of reduced chondrules. Science, 371, 136–139.

Connolly, H.C. and Hewins, R.D. (1996) Constraints on chondrule precursors from experimental data in Chondrules and the protoplanetary disk. In R.H. Hewins, R.H. Jones, and E.R.D. Scott, Eds., Condrules and the protoplanetary disk, p. 13–20. Cambridge University Press, Cambridge, U.K.

Deines, P., Nafziger, R.H., Ulmer, G.C., and Woermann, E. (1974) Temperature-oxygen fugacity tables for selected gas mixtures in the system C-H-O at one atmosphere total pressure. Earth and Mineral Science Exploration Station Bulletin, 88, Pennsylvania State University, University Park.

Doan, A.S., and Goldstein, J.I. (1970) The ternary phase diagram Fe-Ni-P. Metallurgical Transactions, 1, 1759–1767.

Dohmen, R., Chakraborty, S., Palme, H., and Rammensee, W. (1998) Solid-solid reactions mediated by a gas phase: an experimental study of reactions progress and the role of surfaces in the system olivine+iron metal. American Mineralogist, 83, 970–984.

Fei, Y. and Saxena, S.K. (1986) A thermochemical data base for phase equilibria in the system Fe-Mg-Si-O at high pressure and temperature. Physics and Chemistry of Minerals, 13, 311–324.

Goodrich, C.A. (1992) Ureilites: A critical review. Meteoritics, 27, 327–352.

Hanon, P., Robert, F., and Chaussidon, M. (1998) High carbon concentrations in meteoritic chondrules: a record of metal-silicate differentiation. Geochimica et Cosmochimica Acta, 62, 903–913.

Holland, T.J.B. and Powell, R. (1990) An internally consistent thermodynamic dataset with uncertainties and correlations: the system Na_2O-K_2O-CaO-MnO-FeO-Fe_2O_3-Al_2O_3-SiO_2-TiO_2-C-H_2-O_2. Journal of Metamorphic Petrology, 8, 89–124.

Jaoul, O., Houlier, B., Cherghmakani, M., Pichon, R., and Liebermann, R.C. (1987) Surface destabilization and laboratory-induced non-stoichiometry in San Carlos Olivine. Physics and Chemistry of Minerals, 15, 41–53.

Jones, R.H. and Danielson, A. (1997) Chondrule origin for dusty relict olivine in unequilibrated chondrites. Meteoritics Planetary Science, 32, 753–760.

Keller, L.P. and McKay D.S. (1997) The nature and origin of rims on lunar soil grains. Geochimica et Cosmochimica Acta, 61, 2331–2341.

Lemelle, L. (1998) Etude expérimentale de la déstabilisation de l'olivine en milieu réducteur. Applications à la nébuleuse solaire. PhD dissertation, University Denis Diderot (Paris 7), Paris.

Lemelle, L., Guyot, F., Fialin, M., and Pargamin, J. (2001) Experimental study of chemical coupling between reduction and volatilization in olivine single crystals. Geochimica et Cosmochimica Acta, in press.

Mittlefehldt, D.W., McCoy, T.M., Goodrich, C.A., and Kracher A. (1998) Non-chondritic meteorites from asteroidal bodies. In J.J. Papike, Ed., Planetary Materials, 36, 473–4103. Mineralogical Society of America Reviews in Mineralogy, Washington, D.C.

Nagahara, H. (1981) Evidence for secondary origin of chondrules, Nature, 292, 135–136.

Nakamura, A. and Schmalzried, H. (1984) On the Fe^{2+}-Mg^{2+}-Interdiffusion in olivine (II). Berichte der Bunsengeseffschaft für Physikalische Chemie, 88, 140–145.

Nitsan, U. (1974) Stability field of olivine with respect to oxidation and reduction. Journal of Geophysical Research, 79, 706–711.

Rambaldi, E.R. (1981) Relic grains in chondrules. Nature, 293, 558–561.

Sandford, S. (1996) The inventory of interstellar materials available for the formation of the solar system. Meteoritics and Planetary Science, 31, 449–476.

Van Cappellen, E. (1990) The parameterless correction method in X-ray microanalysis. Microscopy, Microanalysis, Microstructures, 1, 1–22.

Van Cappellen, E. and Doukhan, J.C. (1994) Quantitative X-ray microanalysis of ionic compounds. Ultramicroscopy, 53, 343–349.

Wu, T. and Kohlstedt, D.L. (1988) Rutherford Backscattering spectroscopy study of kinetics of oxidation of $(Mg,Fe)_2SiO_4$. Journal of the American Ceramic Society, 71, 540–545.

Zanda, B., Bourot-Denise, M., Perron, C., and Hewins, R. (1994) Origin and metamorphism redistribution of silicon, chromium and phosphorus in the metal of chondrites. Science, 265, 1846–1849.

MANUSCRIPT RECEIVED FEBRUARY 23, 2000
MANUSCRIPT ACCEPTED SEPTEMBER 11, 2000
PAPER HANDLED BY JOHN H. JONES